ECOLE DES MINES DE NANTES

SUBATECH

UMR Université, Ecole des Mines, IN2P3/CNRS

LABORATOIRE DE PHYSIQUE SUBATOMIQUE
ET DES TECHNOLOGIES ASSOCIEES

PARTICLE CORRELATIONS AT ALICE

B. Erazmus, R. Lednicky, V. Lyuboshitz, L. Martin,
K. Mikhailov, J. Pluta, Yu Sinyukov,
A. Stavinsky, K. Werner

Rapport Interne SUBATECH 98-03

4, RUE ALFRED KASTLER BP 20722 44307 NANTES CEDEX 3 TELEPHONE 02 51 85 81 00 TELECOPIE 02 51 85 84 79 E-mail

« FRCPN11 IN2P3 FR

Particle correlations at ALICE

B. Erazmus, R. Lednický[1], V. Lyuboshitz[2], L. Martin, K. Mikhailov[3], J. Pluta, Yu. Sinyukov[4], A. Stavinsky[3], K. Werner
Laboratoire SUBATECH, Université de Nantes / Ecole des Mines de Nantes / IN2P3/CNRS, 4 rue Alfred Kastler, La Chantrerie, 44070 Nantes Cedex 03, France

Abstract

The ability of the ALICE detector for determination of the space-time characteristics of particle production in heavy-ion collisions at LHC from measurements of the correlation functions of identical and nonidentical particles at small relative velocities is discussed. The possibility to use the correlations of nonidentical particles for a direct determination of the delays in emission of various particle species at time scales as small as 10^{-23} s is demonstrated. The influence of the multi-boson effects on pion multiplicities, single-pion spectra and two-pion correlation functions is discussed.

1 Introduction

The correlation function of identical particles with nearby velocities is sensitive to the relative space-time distances between the emission points due to the effects of Bose-Einstein or Fermi-Dirac statistics [1-3] and the strong and Coulomb final state interaction [4-6] The effect of final state interaction allows to obtain similar information also from correlations of nonidentical particles [6]-[8].

It should be stressed that particle correlations at high energies usually measure only a small part of the space-time emission volume since, due to substantially limited decay momenta of few hundred MeV/c, the sources, despite their fast longitudinal motion, emit the correlated particles with nearby velocities mainly at nearby space-time points. The dynamical examples are sources-resonances [9]-[15], colour strings [16, 17], hydrodynamical expansion [18]-[25].

Thus, the features of emitting sources can be investigated in the frame of an approach which includes the dynamics of the emission process as well as the effects of quantum statistics (QS) and final state interactions (FSI) (see Section 5). Different mechanisms are considered in theoretical models: string and colour rope formation, hydrodynamical expansion, resonance production, rescattering, mean field effects etc., and finally the deconfinement transition and the creation of quark-gluon plasma (QGP). It is important that particle correlations contain the information about the dynamical evolution of the emission process, such as proper time of decoupling (freeze-out), duration of particle emission and the presence of collective flows. In particular, the decoupling time and intensity of transversal flows should be closely related to the QGP formation and to the latent heat of the phase transition [18, 20, 22].

[1]Permanent address: Institute of Physics, Na Slovance 2, 18040 Prague 8, Czech Republic
[2]Permanent address: JINR Dubna, P.O.Box 79, Moscow, Russia
[3]Permanent address: ITEP, B. Cheremushkinskaya 25, 117259 Moscow, Russia
[4]Permanent address: Institute for Theoretical Physics of National Acad. Sci., Kiev 252143, Ukraine

It should be emphasized that, depending on the characteristic space-time distance between particle emission points, both Coulomb and nuclear final state interactions can significantly influence the shape of the correlation function of identical particles (e.g., they dominate in the case of two-proton correlations) and they are the main source of correlations of non-identical particles. In particular, the shape of the correlation function of two charged particles (identical or nonidentical) emitted at large relative distances in their c.m.s. is mainly determined by the Coulomb interaction and is increasingly sensitive to this distance with increasing particle masses and charges, i.e. with decreasing Bohr radius of the particle pair (see Sections 7 and 8).

The identical particle interferometry yields an important information on the relative space-time distances between the emission points of the particles of given type. Under certain conditions this relative information can be transformed to the absolute one, such as the decoupling proper time in the case of an expansion process. Measuring the decoupling times for various particle species and assuming the one and the same onset time for all emission processes, we can even estimate the possible delays in the emission of different particles. On the other hand, the correlations of nonidentical particles appear to be directly sensitive to the delays in particle emission and thus can serve as a new source of the important complementary information to the standard interferometry measurements.

In fact, it can be shown [8] that the directional analysis of the correlations of two nonidentical particles, in contrast to the identical ones, allows to measure not only the anisotropy of the distribution of the relative space-time coordinates of the emission points, but also - its asymmetry. In particular, the differences in the mean emission times of various particle species can be directly determined, including their signs (see Sections 3 and 7). This opens a new possibility to determine, in a model independent way, which sort of particles ($K^+, K^-, \pi^+, \pi^-, p...$) was emitted earlier and which later at very short time scales of several fm/c or higher. In particular, this effect could be useful to indicate the formation of QGP. Note that usually kaons are expected to be emitted earlier than pions due to their larger mean free path. In the case of strangeness distillation from the mixed hadronic and QGP phase a delay is expected between the emission of strange and antistrange particles.

Concerning the methodical problems, the correlation function of nonidentical particles, contrary to the case of identical pairs, is practically not influenced by the two-track resolution. The influence of the momentum resolution is expected to be similar as in the case of identical particle interferometry and it should be studied in detail for various particle pairs (see Section 6).

The effect of QS is usually considered in the limit of a low phase-space density such that the possible multi-boson effects can be neglected. This approximation seems to be justified by present experimental data which does not point to any spectacular multi-boson effects neither in single-boson spectra nor in two-boson correlations. Nevertheless, these effects can be of some importance for realistic simulations of heavy ion collisions [26] or they can clearly show up in some rare events or the regions of momentum space in which the pion phase-space density becomes large (see Sections 4 and 9).

2 General formalism

As usual we assume sufficiently small phase-space density of the produced multi-particle system, such that the correlation of two particles emitted with a small relative velocity in nearby space-time points is influenced by the effects of their mutual QS and FSI only. The ideal correlation function $R(p_1, p_2)$ of the two particles is defined as a ratio of their differential production cross section to the reference one which would be observed in the absence of the effects of QS and FSI. In heavy-ion collisions or at sufficiently high energies we can neglect kinematic constraints and most of the dynamical correlations and construct the reference distribution, e.g., with the help of particles from different events.

Assuming the momentum dependence of the one-particle emission probabilities inessential when varying the particle 4-momenta p_1 and p_2 by the amount characteristic for the correlation due to QS and FSI, i.e. assuming that the components of the mean space-time distance between particle sources are much larger than those of the space-time extent of the sources, we get the well-known result of Kopylov and Podgoretsky for identical particles, modified by the substitution of the plane wave $e^{ip_1x_1+ip_2x_2}$ by the non-symmetrized Bethe-Salpeter amplitudes in the continuous spectrum of the two-particle states $\psi^{S(+)}_{p_1p_2}(x_1, x_2)$ [6]. For nonidentical particles

$$R(p_1, p_2) = \sum_S \rho_S \langle |\psi^{S(+)}_{p_1p_2}(x_1, x_2)|^2 \rangle_S, \tag{1}$$

where the averaging should be done over the 4-coordinates $x_i = \{t_i, \mathbf{r}_i\}$ of the emission points of the two particles in a state with total spin S, populated with the probability ρ_S, $\sum_S \rho_S = 1$:

$$\langle f \rangle_S = \int f \cdot D^S_2(p_1, x_1; p_2, x_2)\, d^4x_1\, d^4x_2 / P^S_2(\mathbf{p}_1, \mathbf{p}_2). \tag{2}$$

Here the two-particle emission function D^S_2 is a non-equal time analog of the two-particle Wigner density and

$$P^S_2(\mathbf{p}_1, \mathbf{p}_2) = \int D^S_2(p_1, x_1; p_2, x_2)\, d^4x_1\, d^4x_2 \tag{3}$$

is the normalized to unity momentum distribution of the two uncorrelated (non-interacting) particles. For identical particles, the Bethe-Salpeter amplitude in Eq. (1) should be properly symmetrized:

$$\psi^{S(+)}_{p_1p_2}(x_1, x_2) \to [\psi^{S(+)}_{p_1p_2}(x_1, x_2) + (-1)^S \psi^{S(+)}_{p_2p_1}(x_1, x_2)]/\sqrt{2}. \tag{4}$$

After the separation of the two-particle c.m.s. motion: $\psi^{S(+)}_{p_1p_2}(x_1, x_2) = e^{iPX}\psi^{S(+)}_{\tilde{q}}(x)$, where $X = [(p_1P)x_1 + (p_2P)x_2]/P^2$ and $P \equiv 2p = p_1 + p_2$ are the pair c.m.s. 4-coordinate and its 4-momentum respectively, the Bethe-Salpeter amplitude in Eq. (1) can be substituted by the amplitude $\psi^{S(+)}_{\tilde{q}}(x)$, depending only on the relative 4-coordinate $x \equiv \{t, \mathbf{r}\} = x_1 - x_2$ and the generalized relative 4-momentum $\tilde{q} = q - p(qp)/p^2$, $q = p_1 - p_2$. In the two-particle c.m.s. $\mathbf{p}^*_1 = -\mathbf{p}^*_2 \equiv \mathbf{k}^*$, $\tilde{\mathbf{q}}^* = 2\mathbf{k}^*$, $\tilde{q}^*_0 = 0$. At equal emission times in the two-particle c.m.s. ($t^* = t^*_1 - t^*_2 = 0$) this amplitude coincides with a stationary solution of the scattering problem $\psi^{S(+)}_{-\mathbf{k}^*}(\mathbf{r}^*)$, having at large r^* the asymptotic form of a superposition of the plane and outgoing spherical waves. It can be shown [6] that the amplitude $\psi^{S(+)}_{\tilde{q}}(x)$ can usually be substituted by this solution (*equal time* approximation).

Note that the two-particle correlations are often analyzed in terms of the *out* (x), *side* (y) and *longitudinal* (z) components of the vector $\mathbf{Q} = \{Q_x, Q_y, Q_z\} \equiv 2\mathbf{k}^*$ or - the invariant variable $Q_{inv} = |\mathbf{Q}| \equiv 2k^*$. Here the *out* and *side* denote the transverse, with respect to the reaction axis, components of the vector $\mathbf{Q}$, the *out* direction is parallel to the transverse component of the pair momentum $\mathbf{P}$. Sometimes, to get rid of a fast longitudinal motion of the particle sources, the longitudinally comoving system (LCMS) is introduced. In this system $P_z = 0$ so that the vectors $\mathbf{q}$ and $\mathbf{Q}$ coincide except for the component $q_x = \gamma_\perp Q_x$, where $\gamma_\perp$ is the LCMS Lorentz factor of the pair.

3 Measurements of the delays in particle emission

The correlation function of two nonidentical particles, compared with the identical ones, contains a principally new piece of information on the relative space-time asymmetries in particle emission [8]. In particular, it allows for a measurement of the mean relative delays $\langle t_1 - t_2 \rangle$ in particle emission. This is clearly seen in the case of neutral particles when the two-particle amplitude $\psi^{S(+)}_{-\mathbf{k}^*}(\mathbf{r}^*)$ takes on the form

$$\psi^{S(+)}_{-\mathbf{k}^*}(\mathbf{r}^*) = e^{-i\mathbf{k}^*\mathbf{r}^*} + \phi^S_{k^*}(r^*). \tag{5}$$

Here the scattered wave $\phi^S_{k^*}(r^*)$ is practically independent of the directions of the vectors $\mathbf{k}^*$ and $\mathbf{r}^*$ since we consider sufficiently small momenta k^* of the particles in their c.m.s. so that their interaction is dominated by s-waves. The correlation function in the form

$$\begin{aligned} R(p_1, p_2) &= \sum_S \rho_S \langle |\psi^{S(+)}_{-\mathbf{k}^*}(\mathbf{r}^*)|^2 \rangle_S \\ &= 1 + \sum_S \rho_S \langle |\phi^S_{k^*}(r^*)|^2 + 2\mathrm{Re}\phi^S_{k^*}(r^*) \cos \mathbf{k}^*\mathbf{r}^* - 2\mathrm{Im}\phi^S_{k^*}(r^*) \sin \mathbf{k}^*\mathbf{r}^* \rangle_S \end{aligned} \tag{6}$$

is sensitive to the relative space-time asymmetry due to the odd term $\sim \sin \mathbf{k}^*\mathbf{r}^*$. The sensitivity of the correlation function to the mean relative time delay $\langle t \rangle \equiv \langle t_1 - t_2 \rangle$ in particle emission is clearly seen when considering the behavior of the vector $\mathbf{r}^*$ in the limit $|vt| \gg r$. Making the Lorentz transformation from the rest frame of the source to the c.m.s. of the two particles: $r^*_L = \gamma(r_L - vt)$, $r^*_T = r_T$, we see that, in the considered limit, the vector $\mathbf{r}^*$ is only slightly affected by averaging over the spatial distance $r \ll |vt|$ of the emission points in the rest frame of the source: $\mathbf{r}^* \approx -\gamma \mathbf{v} t$ is nearly parallel or antiparallel to the velocity vector $\mathbf{v}$ of the pair, depending on the sign of the time difference $t \equiv \Delta t = t_1 - t_2$.

For charged particles there arise additional odd terms due to the confluent hypergeometrical function $F(\alpha, 1, z) = 1 + \alpha z/1!^2 + \alpha(\alpha+1)z^2/2!^2 + \ldots$ modifying the plane wave in Eq. (5):

$$\psi^{S(+)}_{-\mathbf{k}^*}(\mathbf{r}^*) = e^{i\delta}\sqrt{A_c(\eta)}[e^{-i\mathbf{k}^*\mathbf{r}^*}F(-i\eta, 1, i\rho) + \phi^S_{ck^*}(r^*)], \tag{7}$$

where $\rho = \mathbf{k}^*\mathbf{r}^* + k^*r^*$, $\eta = (k^*a)^{-1}$, $\delta = \arg\Gamma(1 + i\eta)$ is the Coulomb s-wave phase shift, $A_c(\eta) = 2\pi\eta/[\exp(2\pi\eta) - 1]$ is the modulus squared of the nonrelativistic Coulomb wave function at zero distance and a is the Bohr radius of the two-particle system [5]. Clearly, at a given distance r^*, the effect of the odd component in the Coulomb wave function is of

[5]The exponential function in the Coulomb penetration factor $A_c(\eta)$ is the well-known Gamow factor.

increasing importance with a decreasing Bohr radius of the particle pair, i.e. for particles of greater masses or electric charges.

It is clear that, in the limit $v\langle|t|\rangle \gg \langle r\rangle$, a straightforward way to determine the mean time difference $\langle t\rangle$ is to measure the correlation functions $R_+(\mathbf{k}^*\mathbf{v} \geq 0)$ and $R_-(\mathbf{k}^*\mathbf{v} < 0)$ (see Fig. 1).. Depending on the sign of $\langle t\rangle$, their ratio R_+/R_- should show a peak or a dip in the region of small k^* and approach 1 at large values of k^* [6]. As the sign of the scalar product $\mathbf{k}^*\mathbf{v}$ is practically equal to that of the difference of particle velocities $v_1 - v_2$ (this equality is always valid for particles of equal masses), the sensitivity of the correlation functions R_+ and R_- to the sign of the difference of particle emission times has a simple explanation in terms of the classical trajectory approach (see, e.g., [27]). Clearly, the interaction between the particles in the case of an earlier emission of the faster particle will be weaker compared with the case of its later emission (the interaction time being longer in the latter case leading to a stronger correlation). It means that $|R_+ - 1| < |R_- - 1|$ provided that $\langle t_1 - t_2\rangle < 0$. In particular, in the case of negligible contribution of the strong FSI, when $(R-1)$ is positive\negative for the pairs of particles with unlike\like-sign charges, we may expect that, at $\langle t_1 - t_2\rangle < 0$, the ratio R_+/R_- is lower\higher than unity. Noting that the Bohr "radius" a is negative\positive for the pairs of particles with unlike\like-sign charges, this expectation is in accordance with Eqs. (1) and (7) at $k^* \to 0$, $\langle r^*\rangle \ll |a|$ and $\langle|\phi^S_{ck^*}(r^*)|\rangle \ll 1$. Indeed, taking into account that for the pairs of uncorrelated particles at $k^* \to 0$ the distribution of the vector $\mathbf{k}^*$ approaches the isotropic one,

$$R_+/R_- \approx 1 + 2\frac{\langle r^*_L\rangle}{a} \to 1 - 2\frac{\langle \gamma v(t_1 - t_2)\rangle}{a}, \tag{8}$$

where the arrow indicates the limit $v\langle|t|\rangle \gg \langle r\rangle$.

For practical applications of the method it may be useful to note that the pairs characterized by a small value of the scalar product $\mathbf{k}^*\mathbf{v} = k^* v\cos\psi$ are not sensitive to the asymmetry $\langle r^*_L\rangle$ and to the related mean difference of the emission times $\langle\Delta t\rangle$. Therefore, the method sensitivity can be increased by rejecting the pairs with a small value of $|\cos\psi|$. The optimum cut $|\cos\psi| > 1/3$ corresponds to the enhancement factor $\sqrt{32/27} \doteq 1.09$ in the method sensitivity which is defined as a ratio of the effect to its error. The maximal sensitivity enhancement factor of $\sqrt{4/3} \doteq 1.16$ (35% gain in the statistics) can be obtained by replacing the above sharp angular cut with a weight $|\cos\psi|$ for each pair [7].

4 Multi-boson effects

Since the pions are bosons there can be multi-boson effects enhancing the production of pions with low relative momenta and influencing also the two-pion correlation function. One can even hope to observe new interesting phenomena like Boson condensation or speckles in some rare events or regions of momentum space in which the pion phase-space density f becomes of the order of unity (see, e.g., [3], [28]-[34]).

The mean phase-space density of the pions of a given type in the region of the momentum $\mathbf{p}$ (rapidity y and transverse momentum $\mathbf{p}_t$) can be estimated, in the small density

[6] In the absence of the Coulomb interaction this ratio approaches 1 also at $k^* \to 0$.

[7] It is easy to check that the weight $|\cos\psi|^n$ enhances the method sensitivity by a factor of $(2n+1)^{1/2}/(n/2+1)$. The optimal value of $n = 1$ yields the enhancement factor equal to the maximal possible one, following from the moment or fitting method.

limit, as a number of the pions interfering with a pion of momentum $\mathbf{p}$ [33, 34]:

$$\langle f\rangle_{\mathbf{p}} = \int f^2(\mathbf{x},\mathbf{p})\,d^3\mathbf{r} \,/ \int f(\mathbf{x},\mathbf{p})\,d^3\mathbf{r} \approx \int [R(p_1,p_2)-1] n(\mathbf{p}_1) n(\mathbf{p}_2)\,d^3\mathbf{q} \,/ n(\mathbf{p}), \qquad (9)$$

$\mathbf{q} = \mathbf{p}_1 - \mathbf{p}_2$, $\mathbf{p} = \frac{1}{2}(\mathbf{p}_1 + \mathbf{p}_2)$. Using the usual Gaussian parametrization for the correlation function in the LCMS:

$$R(p_1,p_2) = 1 + \lambda \exp(-r_x^2 q_x^2 - r_y^2 q_y^2 - r_z^2 q_z^2), \qquad (10)$$

where x, y ($\mathbf{y} \parallel \mathbf{z} \times \mathbf{p}$) and z denote the outward, sideward and longitudinal directions respectively and parametrizing the single-particle spectra as

$$n(\mathbf{p}) \equiv \frac{d^3n}{d^3\mathbf{p}} = \frac{dn}{dy} \frac{\exp(-p_t/T)}{2\pi T^2 m_t \cosh y}, \qquad (11)$$

we arrive at the mean pion phase-space density

$$\langle f\rangle_{\mathbf{p}} = \lambda \frac{\sqrt{\pi}}{2} \frac{\exp(-p_t/T)}{VT^2 m_t} \frac{dn}{dy}, \qquad (12)$$

where $V = r_x r_y r_z$ is the interference volume. At SPS energies this quantity is typically ~ 0.1 at $p_t \approx T \approx 200$ MeV/c, $y \approx 0$.

At present energies the interference volume V in LCMS seems to scale with the density dn/dy (see, e.g., [35, 36]) pointing to the freeze-out of the particles at a constant phase-space density. Clearly, if this trend will survive up to the LHC energies then there will be no spectacular multi-boson effects in the ordinary events at ALICE. In such situation the standard two-particle interferometry technique could be used to measure the space-time intervals between the production points. The corresponding interferometric radii for lead-lead collisions at ALICE would be however rather large - about 15-20 fm.

The multi-boson effects can show up in certain classes of events or in some regions of momentum space. Thus a strong transversal flow can lead to rather dense gas of soft pions in the central part of the hydrodynamical tube at the final expansion stage (see, e.g., [21]). Another example is a rapidly expanding system with the entropy much smaller than in the case of total equilibrium. Due to large gradients of temperature or velocity the hydrodynamical layer near the boundary with vacuum can decay at a large phase-space density and lead to pion speckles even at moderate transverse momenta [37].

Because of large interference volumes expected at RHIC and LHC energies one could raise a question about importance of the screening effects on the correlations of charged pions. In fact, below we present arguments showing that the screening will be of minor importance even at LHC. Note that in the scenario with a constant phase-space density the corresponding Debye radius

$$r_D = [4\pi(n_+ + n_-)e^2/T]^{-1/2}, \qquad (13)$$

where $e^2 = 1/137$ and $n_+ + n_-$ is the total density of charged pions in the configuration space, will be also constant, up to a weak energy dependence due to the temperature T. Assuming that pions with a rapidity difference greater than unity come from spatially disjoint regions of phase-space, we can put

$$n_+ = \left(\frac{\lambda}{(2\pi)^3}\right)^{1/2} \frac{dn_+/dy}{V} = \frac{\sqrt{2}}{\sqrt{\lambda}\pi^2} T^3 \langle f_+\rangle_y \qquad (14)$$

and obtain $r_D \approx 15$ fm at $\langle f_+ \rangle_y \approx 0.1$ and $T \approx 200$ MeV/c ($r_D \sim 1/T$). Thus at LHC energies we can expect the characteristic distances between the pion production points comparable or larger than the screening radius r_D leading to a suppression of the usual two-particle Coulomb effects. In fact, two charged pions produced at a distance $r^* > r_D$ start to feel their Coulomb field only after some time when the density decreases to a value corresponding to Debye radius smaller than r^*. During this time the vector of the relative distance between the pion emission points increases approximately by

$$\Delta \mathbf{r}^* = \frac{\mathbf{k}^*}{T} V^{1/3} [\left(\frac{r^*}{r_D}\right)^{2/3} - 1]. \tag{15}$$

Substituting $\mathbf{r}^*$ by $\mathbf{r}^* + \Delta \mathbf{r}^*$ in the argument of the Coulomb wave function, we can see that the suppression of the Coulomb effect can be substantial only in the region of large relative momenta $k^* > T$ where the correlations due to QS and FSI are already negligible.

The multi-boson effects can be practically treated provided that we can neglect particle interaction in the final state and assume independent emission of non-interfering particles (a valid assumption for heavy ion collisions), supplemented by the requirement of a universal one-particle emission function $D(p, x)$, independent of the origin of one-particle sources. We can then write the n-particle emission function as a product of the single-particle ones:

$$D_n(p_1, x_1; p_2, x_2) = \prod_{i=1}^{n} D(p_i, x_i). \tag{16}$$

Then, similar to refs. [31, 32] it is convenient to define

$$\begin{aligned} G_1^{(2)}(\mathbf{p}_1, \mathbf{p}_2) &= \int d^4x D(\frac{p_1 + p_2}{2}, x) \cdot \exp(i(p_1 - p_2)x), \\ G_n^{(2)}(\mathbf{p}_1, \mathbf{p}_2) &= \int d^3\mathbf{k}_2 \ldots d^3\mathbf{k}_n G_1^{(2)}(\mathbf{p}_1, \mathbf{k}_2) \ldots G_1^{(2)}(\mathbf{k}_n, \mathbf{p}_2) \\ &\equiv \int d^3\mathbf{k}_2 G_{n-1}^{(2)}(\mathbf{p}_1, \mathbf{k}_2) G_1^{(2)}(\mathbf{k}_2, \mathbf{p}_2), \\ G_n &= \int d^3\mathbf{p} G_n^{(2)}(\mathbf{p}, \mathbf{p}). \end{aligned} \tag{17}$$

The function $G_1^{(2)}$ at equal momenta is just the original (not affected by the multi-boson effects) single-boson spectrum normalized to unity:

$$P(\mathbf{p}) = G_1^{(2)}(\mathbf{p}, \mathbf{p}), \quad \int d^3\mathbf{p} P(\mathbf{p}) \equiv G_1 = 1. \tag{18}$$

The related quantities are so called cumulants

$$\begin{aligned} K_n^{(2)}(\mathbf{p}_1, \mathbf{p}_2) &= (n-2)! \sum_{i=1}^{n-1} G_i^{(2)}(\mathbf{p}_1, \mathbf{p}_2) G_{n-i}^{(2)}(\mathbf{p}_2, \mathbf{p}_1) / [P(\mathbf{p}_1) P(\mathbf{p}_2)], \\ K_n^{(1)}(\mathbf{p}) &= (n-1)! G_n^{(2)}(\mathbf{p}, \mathbf{p}) / P(\mathbf{p}), \\ K_n &= (n-1)! G_n. \end{aligned} \tag{19}$$

It can be shown that the Bose-Einstein (BE) weight of an event with n identical spin-zero bosons is determined through the cumulants K_j by the recurrence relation [26]:

$$\omega_n = C_0^{n-1} K_1 \omega_{n-1} + C_1^{n-1} K_2 \omega_{n-2} + \ldots + C_{n-1}^{n-1} K_n \omega_0 \tag{20}$$

with $\omega_0 = \omega_1 = 1$; C_i^{n-1} are the usual combinatorial numbers, $C_0^{n-1} = C_{n-1}^{n-1} = 1$. One can check that $\omega_n = n!$ provided that all the elementary one-particle sources are situated at one and the same space-time point so that all the single-boson states are identical and $K_{j+1} = j!$ [8].

The BE affected single- and two-boson spectra, respectively normalized to n and $n(n-1)$, can be written as

$$n_n^{(1)}(\mathbf{p}) = n\omega_n^{(1)}(\mathbf{p}) \cdot P(\mathbf{p})/\omega_n \tag{21}$$

and

$$n_n^{(2)}(\mathbf{p}_1, \mathbf{p}_2) = n(n-1)\omega_n^{(2)}(\mathbf{p}_1, \mathbf{p}_2)P(\mathbf{p}_1)P(\mathbf{p}_2)/\omega_n, \tag{22}$$

where the differential B-E weights $\omega_n^{(1)}(\mathbf{p})$ and $\omega_n^{(2)}(\mathbf{p}_1, \mathbf{p}_2)$ are expressed through the differential cumulants $K_n^{(1)}(\mathbf{p})$ and $K_n^{(2)}(\mathbf{p}_1, \mathbf{p}_2)$:

$$\omega_n^{(1)}(\mathbf{p}) \equiv \int d^3\mathbf{p}'\omega_n^{(2)}(\mathbf{p}, \mathbf{p}')P(\mathbf{p}') = \sum_{j=0}^{n-1} C_j^{n-1} K_{j+1}^{(1)}(\mathbf{p})\omega_{n-1-j},$$

$$\omega_n^{(2)}(\mathbf{p}_1, \mathbf{p}_2) = \sum_{j=0}^{n-2} C_j^{n-2}\omega_{n-2-j}[\sum_{l=0}^{j} C_l^j K_{l+1}^{(1)}(\mathbf{p}_1)K_{j-l+1}^{(1)}(\mathbf{p}_2) + K_{j+2}^{(2)}(\mathbf{p}_1, \mathbf{p}_2)]. \tag{23}$$

The differential weight $\omega_n^{(2)}(\mathbf{p}_1, \mathbf{p}_2)$ can be considered as a two-particle correlation function measuring the BE effect on the original uncorrelated two-particle spectrum $\tilde{n}_n^{(2)}(\mathbf{p}_1, \mathbf{p}_2) = n(n-1)P(\mathbf{p}_1)P(\mathbf{p}_2)$, with the normalization

$$\int d^3\mathbf{p}_1 d^3\mathbf{p}_2 \omega_n^{(2)}(\mathbf{p}_1, \mathbf{p}_2)P(\mathbf{p}_1)P(\mathbf{p}_2) = \omega_n. \tag{24}$$

Usually the correlation function is normalized to unity at a large $|\mathbf{q}|$. Such a normalization is approximately satisfied for the correlation function defined as:

$$R_n(\mathbf{p}_1, \mathbf{p}_2) = n_n^{(2)}(\mathbf{p}_1, \mathbf{p}_2)/\tilde{n}_n^{(2)}(\mathbf{p}_1, \mathbf{p}_2) \equiv \omega_n^{(2)}(\mathbf{p}_1, \mathbf{p}_2)/\omega_n. \tag{25}$$

In practice, the two-particle correlation function is defined through the observable spectra as:

$$R_n(\mathbf{p}_1, \mathbf{p}_2) = c_n n_n^{(2)}(\mathbf{p}_1, \mathbf{p}_2)/[n_n^{(1)}(\mathbf{p}_1)n_n^{(1)}(\mathbf{p}_2)]. \tag{26}$$

Similarly, the (semi-)inclusive correlation function is defined as

$$R(\mathbf{p}_1, \mathbf{p}_2) = c\, n^{(2)}(\mathbf{p}_1, \mathbf{p}_2)/[n^{(1)}(\mathbf{p}_1)n^{(1)}(\mathbf{p}_2)], \tag{27}$$

where

$$n^{(1)}(\mathbf{p}) = \sum_n w(n)n_n^{(1)}(\mathbf{p}), \quad n^{(2)}(\mathbf{p}_1, \mathbf{p}_2) = \sum_n w(n)n_n^{(2)}(\mathbf{p}_1, \mathbf{p}_2) \tag{28}$$

are the corresponding (semi-)inclusive single- and two-particle spectra, $w(n)$ is the normalized multiplicity distribution accounting for the BE effect. Later on, using an analytical

[8] This situation is similar (flat correlation function) though different from the case of the emission of so called coherent bosons for which there is no enhancement factor. In fact, when the one-particle sources become closer and closer, so that their distances are less than the wave length of the emitted bosons, they can no more be considered as independent ones and a multi-particle source of non-interfering bosons has to be introduced [38]. To quantify the transition to the non-interfering bosons a concept of the coherence length can be used [39].

Gaussian model for the emission function, we show that the normalization constant c_n can be expressed through the BE weights as:

$$c_n = n\omega_{n-1}^2/[(n-1)\omega_n\omega_{n-2}] \tag{29}$$

and that $c = 1$ for the inclusive correlation function provided a Poissonian multiplicity distribution of the original uncorrelated bosons.

As one can see from formulae (21)-(23), the multi-boson correlations lead to distortions of the original single- and two-particle distributions. Such distortions are small in the case of interference of only two or three identical particles. However, they can become essential for the events with a large number of identical bosons due to factorially increasing number of the correction terms [29] (see also [3] and [31]). For the processes characterized by a high (> 0.1) phase-space density of the identical bosons at the freeze-out time the multi-boson effects can no more be considered as a correction [29].

To account for the multi-boson symmetrization effect in the event simulators, a phase-space weighting procedure was used with weights in the form of a normalized square of the sum of $n!$ plane waves [29, 30]. This procedure however appears not practical for a large n due to the factorially large number of the terms to be computed to calculate the weight and, due to large weight fluctuations. These fluctuations can be substantially reduced by weighting only in the momentum space. The corresponding BE weights are [26]

$$\omega_n^{(n)}(\mathbf{p}_1, \mathbf{p}_2, \ldots \mathbf{p}_n) = \sum_{\sigma} \prod_{i=1}^{n} F_{i\sigma_i}, \tag{30}$$

where

$$F_{ij} = G_1^{(2)}(\mathbf{p}_i, \mathbf{p}_j)/[P(\mathbf{p}_i)P(\mathbf{p}_j)]^{1/2}. \tag{31}$$

The sum in Eq. (30) is over $n!$ possible permutations σ of the sequence $\{1, 2, \ldots n\}$. On the condition of sufficient smoothness of the single-particle spectra, we can put

$$F_{ij} \doteq \int d^4x D(p_{ij}, x) \cdot \exp(iq_{ij}x) / \int d^4x D(p_{ij}, x), \tag{32}$$

where $p_{ij} = \frac{1}{2}(p_i + p_j)$ and $q_{ij} = p_i - p_j$. This function can then be calculated as suggested in [26]:

$$F_{ij} = \langle \exp(iq_{ij}x_k) \rangle_{\mathbf{p}_{ij}}, \tag{33}$$

where the averaging is done over all simulated phase-space points $\{p_k, x_k\}$ such that $\mathbf{p}_k$ is close to a given 3-momentum $\mathbf{p}_{ij}$. However, there is still the problem with factorially large number of the terms required to calculate the weight according to Eq. (30).

Fortunately, when calculating only single- or two-particle distributions according to Eqs. (21) or (22), this number is strongly reduced (eated by the combinatorial numbers C_j^m in Eqs. (23)). We should however perform integration over momenta of one or more particles to determine the functions G_n and the corresponding integrated cumulants $K_n^{(2)}(\mathbf{p}_1, \mathbf{p}_2)$, $K_n^{(1)}(\mathbf{p})$ and K_n.

The numerical averaging of the cumulants of all orders is a difficult task. In the case of large multiplicities of identical bosons ($n > 20$) this is practically possible in the models with a symmetric emission function (allowing to use a special Monte Carlo technique) [29] or with a simple analytical parametrization of this function [31, 32]. For example,

in ref. [32] the corrections to multiplicity distributions, single-particle spectra and two-particle correlation functions were calculated using the relativistic Bjorken model [40] for the emission function. To compute cumulants up to tenth order, the integration was performed analytically over the space-time coordinates and numerically over the momenta.

Generally, for realistic models used to predict particle production in ultra-relativistic heavy-ion collisions, the numerical limitations allow to determine only a few lowest order cumulants (up to about the fourth order) [26]. Fortunately, since the interferometry measurements point out to the constant pion freeze-out phase-space density of ~ 0.1, the lowest order cumulant approximation appears to be sufficient for present and likely also for future heavy-ion experiments. At the same time, the multi-boson effects appear to be important for realistic simulations of heavy ion collisions. As shown in ref. [26] (see also Section 9), for neutral pions they lead to substantial distortions of the multiplicity distributions (increasing the original mean multiplicity by several tens per cent), of the single-pion spectra (enhancing production of the pions with low p_t and small y) and, to a lesser extent, of the two-pion correlation functions (the correlation function at a given multiplicity becoming lower and wider). For identical charged pions these effects are expected to be suppressed due to the repulsive Coulomb interaction.

5 Simulations

The study of nuclear collisions at ultrarelativistic energies ($E_{\rm cms}$/nucleon $\gg$ 1 GeV) is motivated mainly by the expectation that a thermalized system of quarks and gluons (quark–gluon plasma) is created [41]. There are essentially two directions for modeling such interactions: dynamical and thermal approaches. The former ones refer to string models [42, 43, 44, 45, 46, 47] or related methods [48], supplemented by semihard interactions at very high energies [49, 50, 51, 52]. Here, a well established treatment of hadron-hadron scattering, based on Pomerons and AGK rules [53], is extended to nuclear interactions. Thermal methods [54, 55, 56, 57, 58, 59] amount to assuming thermalization after some initial time τ_0, with evolution and hadronization being mostly based on ideal gas assumptions.

Both methods have serious theoretical drawbacks. Even for nuclei as light as sulfur the string models produce particle densities that high that the hadrons are overlapping. So the independent string model is certainly too simplistic, and also considering secondary interactions as binary collisions among hadrons can theoretically not be justified. On the other hand it is also not realistic to consider a homogeneous plasma occupying the whole available volume, what is assumed in thermodynamic models.

A link between the string model and thermal approaches is provided with VENUS 5 by introducing a completely new approach, more realistic than the previous ones. Based on the string model, one first determines connected regions of high energy density. These regions are referred to as quark matter (QM) droplets. For such regions, the initially produced hadrons serve only as a mean to produce the proper fluctuations in the energy density. Presently, a purely longitudinal expansion of the QM droplets is assumed. Once the energy density falls beyond some critical energy density ε_c, the droplet D decays instantaneously into an n-hadron configuration $K = \{h_1 h_2 \ldots h_n\}$ with a probability proportional to Ω, with Ω representing the microcanonical partition function of an n-hadron system. Due to the huge configuration space, sophisticated methods of statistical

physics [60, 61] have to be employed to solve the problem without further approximations. Details can be found in [62] [9].

Our simulations were performed using the String Model for Ultrarelativistic Hadronic Interactions VENUS (version 5.14) [42, 62]. For practical reasons, the formation of the QM droplets was switched off in the simulations at LHC energies. Although in this case the model is not well suited for the LHC energy region, it provides space-time and momentum space characteristics of the freeze-out points of different particle species, which can be used as a reasonable approximation accounting for the presently known basic features of the multiparticle production, including the fast longitudinal motion of the particle sources and resonance production. Besides, it allows to expand the space-time extent of the production region or introduce the shifts in emission times of various particle species and thus to test the possibility to observe such phenomena in the ALICE experiment.

The two–particle correlation functions are calculated by weighting the simulated particle pairs according to Eq. (1). Instead of the 6-dimensional correlation function $R(p_1, p_2)$ we calculate the 1-dimensional one integrating over the single-particle spectra:

$$R(k^*) = \frac{1}{N(k^*)} \sum_{i=1}^{N(k^*)} \sum_S \rho_S |\psi^{S(+)}_{p_{1_i} p_{2_i}}(x_{1_i}, x_{2_i})|^2, \tag{34}$$

where $N(k^*)$ is the number of generated particle pairs in a given k^* bin. In the considered case of unpolarized particles with spins s_1 and s_2, the population probability of the spin-S states is $\rho_S = (2S+1)/[(2s_1+1)(2s_2+1)]$.

6 Experimental resolution

Experimental resolution has been introduced in the simulations using a program based on parametrizations of the full detector simulation [63]. A realistic geometry (beam pipe, ITS active and inactive material, inner vessel, TPC field cage, TPC gas,...) of the ALICE central barrel has been taken into account according to our present knowledge.

This program does include contributions due to multiple scattering, measurement precision and detector alignment and fluctuation in energy loss. Over most of the momentum range the resolution is dominated by multiple scattering. At low transverse momentum, it increases as $1/\beta$ implying an improvement of the resolution with increasing momentum and with decreasing particle mass. The momentum resolution is estimated to be of the order of a few per cent for pions and significantly worse for kaons and protons. The expected angular resolution is of the order of a few mrad in both the polar and the azimuthal directions. One should note that in these simulations the two-track resolution was not accounted for. However, it is expected to have rather small effect even on correlation functions of like charged particles (it will lead to a fraction of unresolved particle pairs with near-by momenta) and practically no effect on unlike particle correlations at small relative velocities.

The effect of the experimental resolution on the relative momentum is summarized in Table 1. One can see from the table:

1) The resolution depends on particle species in accordance with the single-particle momentum resolution which is the best for pions and the worst for protons.

[9] WARNING: VENUS 5 is still in an experimental stage, an official version has not yet been released. It should only be used in a close collaboration with the author.

Table 1: The ALICE resolution: $\sigma(Q_i - Q_i^{'})$, MeV/c. The cut $Q_{inv} < 0.05 GeV/c$ has been applied.

Particles	Q_{side}	Q_{out}	Q_{long}	Q_{inv}
$\pi^+\pi^+, \pi^+\pi^-$	0.3	3.8	0.7	1.2
π^+K^+, π^+K^-	0.4	4.0	1.1	1.8
π^+p, π^-p	0.4	3.9	1.3	2.0
K^+K^+, K^+K^-	0.5	6.5	2.6	3.6
K^+p, K^-p	0.6	8.2	3.2	4.8
pp	0.6	11.6	5.0	6.0

2) The resolution depends on the relative momentum components but for each component it is sufficient to resolve the correlation effect expected in an interval of $Q < 10$ MeV/c. It means that source space-time measurements will be possible at ALICE for all the particle species. The distortion of the correlation functions will be mainly due to Q_{out} component and should be taken into account.

7 Correlations of identical particles

The relative importance of the three factors:

- the quantum statistics,
- the strong interaction and
- the Coulomb interaction,

will be different for different particle species. For instance, for a not too large source, the correlations of protons are dominated by the effect of the strong and Coulomb interaction, while the correlations of charged identical pions are dominated by the effect of quantum statistics. In Fig. 2 we show the two-particle correlation functions for pions, kaons and protons calculated taking into account the effects of quantum statistics and final state, Coulomb and nuclear, interactions. It should be emphasized that for the large systems, expected at LHC energies, the usual Gamow correction substantially deviates from the true Coulomb effect and leads to a big overestimation of the two-pion correlation function compared with that including the effect of quantum statistics only.

It is seen that, in the case of large effective source sizes, the correlations of two protons are, due to their relatively small Bohr radius of 58 fm, stronger than those of pions and kaons.

The correlation functions are only weakly affected by the experimental resolution effects (Fig. 2).

To test the sensitivity of the charged particle correlations to the effective source size, we have introduced different scale factors (2 and 4) to space-time freeze-out coordinates

provided by VENUS (left side of Fig. 3). We can see that for the sizes expected in the ALICE experiment this sensitivity is rather good.

8 Correlations of nonidentical particles

A noticeable sensitivity to the space–time characteristics of the particle emission in the ALICE conditions is also seen in the correlation functions of unlike charged mesons (right side of Fig. 3). However, as already discussed in Section 3, the main interest in the correlations of nonidentical particles is due to the fact that they offer a possibility to measure the space–time asymmetries in their production, in particular, the relative shifts in their mean emission times. To achieve this goal, the correlation function has to be measured in different intervals of the scalar product $\mathbf{k}^*\mathbf{v}$. The simplest way is to measure the correlation functions R_+ and R_-, corresponding to the positive and negative values of $\mathbf{k}^*\mathbf{v}$, respectively (see Fig. 1) [8].

First of all we have tested that the experimental resolution itself cannot simulate the effect of the space–time asymmetry in the R_+/R_- ratio. We have used for this test $\pi^+\pi^-$ pairs which have practically symmetric distribution of the relative 4-coordinates of their emission points. As expected the corresponding R_+/R_- ratio does not deviate from unity within the errors.

In contrast to the unlike pions, VENUS simulation yields noticeable asymmetries in the distribution of the relative 4-coordinates of the pion and proton emission points. In particular, protons are emitted in the mean by 1.3 fm/c later than pions. On the absence of the spatial asymmetries this delay would lead, for the π^+p pairs, to the R_+/R_- ratio greater than unity at small values of k^*. However, Fig. 4 indicates the opposite behavior. It means that the effect seen in this figure is dominated by the negative spatial asymmetry $\langle\Delta r_L\rangle < 0$ overcompensating the effect of the negative time asymmetry $\langle\Delta t\rangle < 0$ in $\langle r_L^*\rangle = \gamma(\langle\Delta r_L\rangle - v\langle\Delta t\rangle)$.

In Fig. 4 we also illustrate the effect of the size–dependence, introducing the scale-factor of 3 to the simulated 4-coordinates of the particle emission points. One can see that with the increasing space–time extent of the source the effect becomes more weak (due to vanishing of the FSI effect) except for a narrowing region near $k^* = 0$ whose depth increases. The latter observation is in agreement with the fact that, in the case of a negligible effect of the strong FSI and at $\langle r^*\rangle \ll |a|$, the deviation from unity of the intercept of the R_+/R_- ratio increases with the increasing asymmetry $\langle r_L^*\rangle$ (see Eq. (8)).

The scaling of the effect with the space–time asymmetry is clearly demonstrated in Fig. 5 for the K^+K^- system by means of adding a value of 10 and -5 fm/c to the K^+ emission time.

The scaling of the effect with the inverse Bohr radius is illustrated in Fig. 6 for the like- and unlike-sign πK, πp and Kp systems (the corresponding Bohr radii $a = \pm 248.5$, ± 225.5 and ± 83.6 fm, respectively). To demonstrate the possibility of a study of the time–delay effect event–by–event, we have calculated here the correlation functions for the πK and πp systems using one simulated event only.

From the remarkable effects seen in Figs. 5 and 6 we can conclude that the R_+/R_- ratio can be sensitive to the shifts in the particle emission times of the order of few fm/c.

9 Analytical model for the multi-boson effects

To illustrate the multi-boson effects in a dense pion gas we use a simple model assuming independent particle emission (see Eq. (16) for the two-particle case) with the Gaussian ansatz for the single-boson emission function $D(p,x)$ [31]:

$$D(p,x) = \frac{1}{(2\pi r_0\Delta)^3}\exp(-\frac{\mathbf{p}^2}{2\Delta^2} - \frac{\mathbf{r}^2}{2r_0^2})\delta(t). \tag{35}$$

Note that this ansatz corresponds to the independent one-particle sources of Kopylov and Podgoretsky, all of the same type, characterized by a universal size of $\sim 1/\Delta$, with the centers distributed according to a Gaussian of a dispersion $\tilde{r}_0^2 = r_0^2 - (2\Delta)^{-2}$. Then, in the low density limit but regardless of the validity of the *smoothness* condition $\tilde{r}_0 \gg 1/\Delta$ (see, however, the footnote after Eq. (20) concerning the independence assumption), the correlation function of two non-interacting identical particles measures the dispersion of the relative 4-coordinates $\tilde{x}$ of the centers of the one-particle sources [3]. For spin-0 bosons

$$R(\mathbf{p}_1,\mathbf{p}_2) = 1 + \langle\cos(q\tilde{x})\rangle = 1 + \exp(-\tilde{r}_0^2\mathbf{q}^2). \tag{36}$$

In this model the original boson phase-space density (not affected by the BE effect) is given by

$$f_n(\mathbf{p},\mathbf{x}) = \frac{n}{(r_0\Delta)^3}\exp(-\frac{\mathbf{p}^2}{2\Delta^2} - \frac{\mathbf{x}^2}{2r_0^2}). \tag{37}$$

The mean densities at a fixed boson momentum $\mathbf{p}$ and averaged over all phase-space are

$$\langle\tilde{f}_n\rangle_{\mathbf{p}} \equiv \int d^3\mathbf{x}(\tilde{f}_n)^2 \,/\, \int d^3\mathbf{x}\tilde{f}_n = \frac{n}{(\sqrt{2}r_0\Delta)^3}\exp(-\frac{\mathbf{p}^2}{2\Delta^2}) \tag{38}$$

and

$$\langle\tilde{f}_n\rangle \equiv \int d^3\mathbf{x}d^3\mathbf{p}(\tilde{f}_n)^2 \,/\, \int d^3\mathbf{x}d^3\mathbf{p}\tilde{f}_n = n/(2r_0\Delta)^3, \tag{39}$$

respectively. Similarly, the original inclusive densities $\tilde{f}(\mathbf{p},\mathbf{x})$, $\langle\tilde{f}\rangle_{\mathbf{p}}$ and $\langle\tilde{f}\rangle$ are given by Eqs. (37)-(39) with the multiplicity n substituted by the original mean multiplicity.

It is important that the Gaussian ansatz in Eq. (35) allows to express $G_n^{(2)}(\mathbf{p}_1,\mathbf{p}_2)$ and G_n in simple analytical forms:

$$\begin{aligned} G_n^{(2)}(\mathbf{p}_1,\mathbf{p}_2) &= (2\pi\Delta^2 A_n)^{-3/2}\exp(-b_n^+(\mathbf{p}_1+\mathbf{p}_2)^2 - b_n^-(\mathbf{p}_1-\mathbf{p}_2)^2) \\ &\to \beta^{-n}\left(\frac{r_0}{\pi\Delta}\right)^{3/2}\exp\left(-\frac{r_0}{4\Delta}(4\mathbf{p}^2+\mathbf{q}^2)\right), \\ G_n &= 1/(8\Delta^2 A_n b_n^+)^{3/2} \to \beta^{-n}, \end{aligned} \tag{40}$$

where A_n, b_n^+ and b_n^- are given by the recurrence relations:

$$\begin{aligned} A_n &= 2\Delta^2 A_{n-1}(b_{n-1}^+ + b_{n-1}^- + b_1^+ + b_1^-) \to \beta^{2n/3}/(2r_0\Delta), \\ 1/b_n^+ &= 1/(b_{n-1}^+ + b_1^+) + 1/(b_{n-1}^- + b_1^-) \to 4\Delta/r_0, \\ b_n^- &= b_1^+ b_1^-/b_n^+ \to b_n^+, \end{aligned} \tag{41}$$

with $A_1 = 1$, $b_1^+ = 1/(8\Delta^2)$ and $b_1^- = r_0^2/2$. Hereafter the arrows indicate the limits of large $n \gg r_0\Delta$; the parameter

$$\beta = (r_0\Delta + 1/2)^3 \tag{42}$$

characterizes the phase-space volume. Using the large-n behavior of the parameters G_n, we can get from the recurrence relation (20) the following large-n limit of the BE weight:

$$\omega_n \to c(\beta) n!/\beta^n, \tag{43}$$

where $c(\beta)$ is a function factorially increasing with β, $c(1) = 1$ [10]. It is worth noting that the large-n limits become equalities at $\beta = 1$ ($r_0\Delta = 1/2$) when $G_n = A_n = 1$, $K_n = (n-1)!$, $\omega_n = n!$ and $b_n^- = b_n^+ = r_0/(4\Delta)$. Recall that $\beta = 1$ corresponds to the minimal possible phase-space volume when all the particle emitters are situated at one and the same space-time point so that the size of the elementary source determines not only the width of the single-particle spectrum but also the characteristic distance between the production points (see however the footnote after Eq. (20) and also ref. [26] for a more detailed discussion). Then $\tilde{r}_0 = 0$ and the correlation function equals 2 for any value of $\mathbf{q}$.

For the multiplicity distribution accounting for the BE effect, assuming the original Poissonian one with the mean multiplicity η: $\tilde{w}(n) = \mathrm{e}^{-\eta}\eta^n/n!$, we get:

$$w(n) = \mathrm{const} \cdot \omega_n \eta^n/n! \to \mathrm{const}' \cdot \xi^n, \quad \xi = \eta/\beta. \tag{44}$$

Comparing the quantity $\xi = \eta/\beta$ with the original inclusive phase-space density $\langle \tilde{f} \rangle = \eta/(2r_0\Delta)^3$ (see Eq. (39)), we can identify ξ as a ratio $\langle \tilde{f} \rangle_{cor}/\langle \tilde{f} \rangle_{cr}$ of the original density corrected for the finite size effects: $\langle \tilde{f} \rangle_{cor} = \langle \tilde{f} \rangle \cdot [1 + 1/(2r_0\Delta)]^3$ and the critical original density $\langle \tilde{f} \rangle_{cr} = 1/8$ corresponding to the explosion of the multiplicity distribution. Taking 0.1 as an estimate of the inclusive phase-space density from AGS and SPS experiments, we get $\xi \approx 0.8$.

The large-n behavior of the multiplicity distribution in Eq. (44) indicates that it approaches the BE one $w_{\mathrm{BE}}(n) = \nu^n/(1+\nu)^{n+1}$ with the mean multiplicity $\nu = \xi/(1-\xi)$. This is demonstrated in Figs. 7 and 8. Thus, at $r_0 = 2.1$ fm and $\Delta = 0.25$ GeV/c, the BE effect transforms the original Poissonian multiplicity distribution with $\eta = 30$ (dotted line in Fig. 7a) to the one with much higher mean and dispersion values (solid line in Fig. 7a). The exponential tail expected for the BE distribution is clearly seen in Fig. 7b where the results are presented in logarithmic scale for $\eta = 10$, $\Delta = 0.25$ GeV/c and $r_0 = 1.5$ fm. The slope parameter b in the exponential fit $w(n) = \mathrm{const} \cdot \exp(-bn)$ of this tail at large n should be, according to Eq. (44), only a function of the variable ξ: $b = -\ln(\xi)$. Such a scaling is demonstrated in Fig. 8a for various values of η, Δ and r_0. Note that $\xi = 0.95$ and 0.72 for Figs. 7a and 7b, corresponding to $b = 0.02$ and 0.27, respectively [11]. Fig. 8c demonstrates the approach of the mean multiplicity $\langle n \rangle$ to the scaling value $\xi/(1-\xi)$, though only for ξ very close to the explosion point $\xi = 1$ ($\xi > 0.99$). Instead, in the region of $\xi < 0.9$, containing the point $\xi \approx 0.8$ indicated by present experiments, we can see an approximate ξ-scaling of the ratio $\langle n \rangle/\eta$ (Fig. 8b).

Note that the approximate ξ-scaling gives a possibility to overcome technical problems with factorially large numbers at high multiplicities. Thus some quantities can be calculated at small or moderate values of η or n and then rescaled to a large one provided the density parameter $\xi = \eta/\beta$ or $\xi_n = n/\beta$ is keeped the same.

[10] A good approximation is $c(\beta) \doteq \beta^{d(\beta)}$, $d(\beta) = a_1 + a_2\beta^{a_3}$, $a_1 = 0.617$, $a_2 = 0.621$ and $a_3 = 0.788$.

[11] At the explosion point $\xi = 1$ the tail of the multiplicity distribution becomes a constant ($b = 0$) so that the mean multiplicity $\langle n \rangle$ would go to infinity provided that there are no energy-momentum constraints. Note that the corresponding critical original mean multiplicity $\eta_{cr} = \beta \equiv (r_0\Delta + 1/2)^3$ is close but different from that given in Eq. (9) of ref. [31].

Regarding the influence of the BE effect on the single-boson spectrum, it can be seen from Eqs. (19)-(21) and (40) that, at sufficiently large momenta when the local density $\langle f_n \rangle_{\mathbf{p}}$ remains small even at large n, this spectrum is dominated by the n-independent contribution $\beta P(\mathbf{p})$ of the original spectrum, otherwise, at large local densities, it is determined by the asymptotic large-density spectrum

$$n_n^{(1)}(\mathbf{p}) \to n \left(\frac{r_0}{\pi\Delta}\right)^{3/2} \exp\left(-\frac{r_0}{\Delta}\mathbf{p}^2\right) \equiv nP_\infty(\mathbf{p}), \tag{45}$$

corresponding to the asymptotic (large-n) value $b_\infty^+ = b_\infty^- = r_0/(4\Delta)$ of the parameters $b_n^\pm$. Note that $P_\infty(\mathbf{p})$ is normalized to unity and that, at $\beta = 1$, it coincides with the original distribution $P(\mathbf{p})$. Similarly, the inclusive single-boson spectrum at small local densities tends to $\eta P(\mathbf{p})$ and, at large ones, it approaches the asymptotic high-density spectrum (see Eq. (52) below):

$$n^{(1)}(\mathbf{p}) \to \langle n \rangle P_\infty(\mathbf{p}). \tag{46}$$

The transfer of the original spectrum to the high-density one is demonstrated for the inclusive distribution in Fig. 9a and, more clearly, for ξ closer to the explosion point $\xi = 1$, in Fig. 9b [12]. In Fig. 9 we also compare the inclusive single-boson spectra with a simple approximation:

$$n^{(1)}(\mathbf{p}) = \eta P(\mathbf{p}) + \frac{\xi}{1-\xi} P_\infty(\mathbf{p}). \tag{47}$$

A good agreement can be seen, except for the region of intermediate momenta narrowing with the increasing density. Experimentally the effect of BE "condensate" was searched for at SPS CERN as a low-p_t enhancement, however, with rather uncertain results (see, e.g., [41]).

In Fig. 10 we show the ratio of the single-particle spectrum to the dominant large-p contribution $\beta P(\mathbf{p})$ of the original spectrum calculated at $\mathbf{p} = 0$ as a function of ξ_n for various multiplicities n. An approximate ξ_n-scaling is seen up to ξ_n of the order of unity. At larger ξ_n this ratio approaches the limit $(2r_0\Delta)^{3/2}\xi_n$ which no more scales with ξ_n. What scales at large ξ_n is not the ratio of the two contributions but the ratio of their integrals, the limiting value of which is just equal to ξ_n (see the corresponding curves in Fig. 10b).

Consider now the correlation function defined in Eq. (26). To determine the normalization constant c_n, it is convenient to rewrite the single- and two-boson spectra at a fixed multiplicity n as

$$\begin{aligned} n_n^{(1)}(\mathbf{p}) &= \sum_{j=0}^{n-1} w(n-1-j)\tilde{G}_{j+1}^{(2)}(\mathbf{p},\mathbf{p})/w(n), \\ n_n^{(2)}(\mathbf{p}_1,\mathbf{p}_2) &= \sum_{j=0}^{n-2} w(n-2-j) \sum_{l=0}^{j} [\tilde{G}_{l+1}^{(2)}(\mathbf{p}_1,\mathbf{p}_1)\tilde{G}_{j-l+1}^{(2)}(\mathbf{p}_2,\mathbf{p}_2) + \\ &\qquad \tilde{G}_{l+1}^{(2)}(\mathbf{p}_1,\mathbf{p}_2)\tilde{G}_{j-l+1}^{(2)}(\mathbf{p}_2,\mathbf{p}_1)]/w(n), \end{aligned} \tag{48}$$

[12] These results agree with those obtained in refs. [31, 32] (see also [34, 26] and references therein) except for a wrong conclusion in [31] that the width of the narrow peak due to the BE "condensate" is of $1/r_0$.

where $w(n)$ is defined in Eq. (44) (it coincides with the multiplicity distribution in the originally Poissonian case) and $\tilde{G}_i^{(2)}(\mathbf{p}_1,\mathbf{p}_2) = \eta^i G_i^{(2)}(\mathbf{p}_1,\mathbf{p}_2)$. Noting further that b_n^+ approaches the limiting value $b_\infty = r_0/(4\Delta)$ from below, while b_n^- does it from above, we can see from Eq. (40) that, at large q, all terms in Eqs. (48) for $n_n^{(1)}(\mathbf{p}_{1,2})$ and $n_n^{(2)}(\mathbf{p}_1,\mathbf{p}_2)$ ($\mathbf{p}_{1,2} = \mathbf{p} \pm \mathbf{q}/2$) can be neglected except for those containing the lowest slope b_1^+. For the normalization constant $c_n = \lim_{q\to\infty}[n_n^{(1)}(\mathbf{p}_1)n_n^{(1)}(\mathbf{p}_2)/n_n^{(2)}(\mathbf{p}_1,\mathbf{p}_2)]$ in Eq. (26) for the correlation function we thus get

$$c_n = [w(n-1)]^2/[w(n)w(n-2)] \equiv n\omega_{n-1}^2/[(n-1)\omega_n\omega_{n-2}]. \tag{49}$$

It follows from Eqs. (26) and (40)-(49) that, for a given multiplicity n, the correlation function intercept $R_n(0)$ decreases and the correlation function width increases with the increasing n or decreasing momentum p, both corresponding to the increasing local density. The well known [29, 30, 31] lowering and widening of the correlation function with the increasing multiplicity is demonstrated, in the considered model, in Fig. 11.

In Fig. 12 we show the intercept as a function of the density parameter ξ_n for two values of the mean momentum: $p = 0$ and 0.2 GeV/c. We can see that the intercept decrease is slower in the latter case, in accordance with a lower local density at higher p.

Regarding the (semi-)inclusive single- and two-boson spectra, they can be written in a form similar to Eqs. (48) only in the originally Poissonian case:

$$\begin{aligned} n^{(1)}(\mathbf{p}) &= \sum_n \sum_{j=0}^{n-1} w(n-1-j)\tilde{G}_{j+1}^{(2)}(\mathbf{p},\mathbf{p})/\sum_n w(n), \\ n^{(2)}(\mathbf{p}_1,\mathbf{p}_2) &= \sum_n \sum_{j=0}^{n-2} w(n-2-j)\sum_{l=0}^{j}[\tilde{G}_{l+1}^{(2)}(\mathbf{p}_1,\mathbf{p}_1)\tilde{G}_{j-l+1}^{(2)}(\mathbf{p}_2,\mathbf{p}_2) + \\ &\qquad \tilde{G}_{l+1}^{(2)}(\mathbf{p}_1,\mathbf{p}_2)\tilde{G}_{j-l+1}^{(2)}(\mathbf{p}_2,\mathbf{p}_1)]/\sum_n w(n). \end{aligned} \tag{50}$$

The normalization constant in Eq. (27) for the (semi-)inclusive correlation function is then

$$c = [\sum_n w(n-1)]^2/[\sum_n w(n)\sum_n w(n-2)]. \tag{51}$$

Clearly, in the completely inclusive case (when $\sum_n w(n-j) = 1$), we have $c = 1$ and

$$\begin{aligned} n^{(1)}(\mathbf{p}) &= \sum_{j=0}^{\infty} \tilde{G}_{j+1}^{(2)}(\mathbf{p},\mathbf{p}), \\ n^{(2)}(\mathbf{p}_1,\mathbf{p}_2) &= \sum_{j=0}^{\infty}\sum_{l=0}^{j}[\tilde{G}_{l+1}^{(2)}(\mathbf{p}_1,\mathbf{p}_1)\tilde{G}_{j-l+1}^{(2)}(\mathbf{p}_2,\mathbf{p}_2) + \tilde{G}_{l+1}^{(2)}(\mathbf{p}_1,\mathbf{p}_2)\tilde{G}_{j-l+1}^{(2)}(\mathbf{p}_2,\mathbf{p}_1)] \\ &\equiv n^{(1)}(\mathbf{p}_1)n^{(1)}(\mathbf{p}_2) + \sum_{j=0}^{\infty}\sum_{l=0}^{j}\tilde{G}_{l+1}^{(2)}(\mathbf{p}_1,\mathbf{p}_2)\tilde{G}_{j-l+1}^{(2)}(\mathbf{p}_2,\mathbf{p}_1) \end{aligned} \tag{52}$$

so that

$$R(\mathbf{p}_1,\mathbf{p}_2) = 1 + \sum_{l=0}^{j}\tilde{G}_{l+1}^{(2)}(\mathbf{p}_1,\mathbf{p}_2)\tilde{G}_{j-l+1}^{(2)}(\mathbf{p}_2,\mathbf{p}_1)/\sum_{l=0}^{j}\tilde{G}_{l+1}^{(2)}(\mathbf{p}_1,\mathbf{p}_1)\tilde{G}_{j-l+1}^{(2)}(\mathbf{p}_2,\mathbf{p}_2) \tag{53}$$

with the intercept $R(0) = 2$ - the result which is generally valid for thermalized systems [34].

It follows from Eqs. (40) and (52) that at sufficiently large momenta, when the local density $\langle f \rangle_{\mathbf{p}}$ remains small even at $\xi \to 1$, the inclusive single-boson spectrum is dominated by the contribution $\eta P(\mathbf{p}) \equiv \tilde{G}_1^{(2)}(\mathbf{p}, \mathbf{p})$ of the original spectrum, otherwise, at large local densities, it approaches the asymptotic large-density ($\xi \to 1$) spectrum in Eq. (46) (see Fig. 9).

Regarding the two-boson spectrum, it is easy to see from Eqs. (40) and (52) that at large local densities it approaches twice the product of the single-boson spectra so that the inclusive correlation function tends to the limiting value of 2. The corresponding increase of the width of the correlation function with the increasing density parameter ξ is demonstrated in Fig. 13.

It should be noted that Eqs. (52) and (53) assume the original Poissonian multiplicity distribution for any arbitrarily large number of bosons. In reality, however, this number is limited due to the finite available energy. It is therefore interesting to see how fast the semi-inclusive spectra approach the inclusive limit with the increasing number n_{max} of the included pions. In Fig. 14 we demonstrate the n_{max}-dependence of the semi-inclusive correlation functions for a fixed value of the density parameter $\xi = 0.95$ and, in Fig. 15 - the n_{max}-dependence of the correlation function intercepts for different ξ-values. We can see that the width of the semi-inclusive correlation function increases with the increasing n_{max}, while its intercept decreases at small n_{max}, reaching a minimum at $n_{max} \approx \langle n \rangle$, and then approaches the limiting value of 2 roughly as $\log n_{max}$. The inclusive behavior is practically saturated at a not very large number of the included pions $n_{max} \approx 5\langle n \rangle$, thus justifying the neglect of the energy-momentum constraints in Eqs. (52) and (53).

The results of the considered simple model should not be taken, however, too literally since: a) in contradiction with the experimental indications on a constant freeze-out phase-space density, in the model there is no correlation between the emission volume and pion multiplicity; b) the static character of the model is justified in a limited rapidity region only.

10 Conclusion.

We have demonstrated the ability of the ALICE detector for determination of the space-time characteristics of particle production in heavy-ion collisions at LHC from measurements of the correlation functions of identical and nonidentical particles at small relative velocities.

We have shown that unlike particle correlations, compared with those of identical particles, contain a principally new piece of information on the relative space-time asymmetries in particle emission, thus allowing, in particular, a measurement of the mean relative delays in particle emission at time scales as small as 10^{-23} s. To determine these asymmetries, the unlike particle correlation functions R_+ and R_- have to be studied separately for positive and negative values of the projection of the relative momentum vector in pair c.m.s. on the pair velocity vector or, generally, - on any direction of interest. The results of simulations of a number of two-particle systems, using the event generator VENUS adapted somewhat arbitrarily for LHC conditions and including the expected resolution of the ALICE detector, demonstrated that the R_+/R_- ratio is sufficiently sensitive to the relative time delays of a few fm/c.

The influence of the multi-boson effects on boson multiplicities, single-boson spectra

and two-boson correlations, including an approximate scaling behavior of some of their characteristics with the phase-space density, has been demonstrated using the simple analytically solvable Gaussian model. Though these effects are hardly to be observable in typical events of heavy ion collisions in present and perhaps also in future heavy-ion experiments, they can clearly show up in some rare events or - in the regions of momentum space with a large pion phase-space density.

References

[1] G. Goldhaber et al., *Phys. Rev.* **120** (1960) 300.

[2] G.I. Kopylov, M.I. Podgoretsky, *Yad. Fiz.* **15** (1972) 392; G.I. Kopylov, *Phys. Lett.* **B50** (1974) 472;

[3] M.I. Podgoretsky, *Fiz. Elem. Chast. Atom. Yad.* **20** (1989) 628 (*Sov. J. Part. Nucl.* **20** (1989) 266).

[4] S.E. Koonin, *Phys. Lett.* **B70** (1977) 43.

[5] M. Gyulassy, S.K. Kauffmann, L.W. Wilson, *Phys. Rev.* **C20** (1979) 2267.

[6] R. Lednicky, V.L. Lyuboshitz, *Yad. Fiz.* **35** (1982) 1316 (*Sov. J. Nucl. Phys.* **35** (1982) 770); Proc. Int. Workshop on Particle Correlations and Interferometry in Nuclear Collisions, CORINNE 90, Nantes, France, 1990 (ed. D. Ardouin, World Scientific, 1990) p. 42; JINR report P2-546-92 (1992) 1; *Heavy Ion Physics* **3** (1996) 93.

[7] D.H. Boal, J.C. Shillcock, *Phys. Rev.* **C33** (1986) 549.

[8] R. Lednicky, V.L. Lyuboshitz, B. Erazmus, D. Nouais, *Phys. Lett.* **B373** (1996) 30; Report SUBATECH 94-20, Nantes 1994.

[9] V.G. Grishin, G.I. Kopylov, M.I. Podgoretsky, *Yad. Fiz.* **13** (1971) 1116.

[10] G.H. Thomas, *Phys. Rev.* **D15** (1977) 2636.

[11] P. Grassberger, *Nucl. Phys.* **B120** (1977) 231.

[12] B.V. Batyunya et al. (LUDMILA), *Yad. Fiz.* **27** (1978) 1556; R. Lednicky, Proc. III Europ. Symp. on Antinucl. Nucleon Int., Stockholm, 1976, *Wenner-Gren* **29** (1977) 477.

[13] B.V. Batyunya et al. (LUDMILA), *Czech. J. Phys.* **31** (1981) 475; R. Lednicky, JINR B2-3-11460, Dubna, 1978.

[14] R. Lednicky, M.I. Podgoretsky, JINR P2-12302, Dubna, 1979; JINR P2-82-327, Dubna, 1982.

[15] R. Lednicky, T.B. Progulova, *Z. Phys.* **C55** (1992) 295.

[16] M.G. Bowler, *Z. Phys.* **C29** (1985) 617.

[17] B. Andersson, W. Hofmann, *Phys. Lett.* **B169** (1986) 364.

[18] S. Pratt, *Phys. Rev. Lett.* **53** (1984) 1219; *Phys. Rev.* **D33** (1986) 1314; S. Pratt, T. Csorgo, J. Zimanyi, *Phys. Rev.* **C42** (1990) 2646.

[19] K. Kolehmainen, M. Gyulassy, *Phys. Lett.* **B130** (1986) 203.

[20] A.N. Makhlin, Yu.M. Sinyukov, *Yad. Fiz.* **46** (1987) 637; *Z. Phys.* **C39** (1988) 69; Yu.M. Sinyukov, *Nucl. Phys.* **A498** (1989) 151c.

[21] S.V.Akkelin, Yu.M. Sinyukov, *Phys. Lett.* **B356** (1995) 525.

[22] G. Bertsch, M. Gong, M. Tohyama, *Phys. Rev.* **C37** (1988) 1896.

[23] Y. Hama, S.S. Padula, *Phys. Rev.* **D37** (1988) 3237.

[24] U. Mayer, E. Schnedermann, U. Heinz, *Phys. Lett.* **B294** (1992) 69.

[25] B.R. Schlei, U. Ornik, M. Plumer, R.M. Weiner, *Phys. Lett.* **B293** (1992) 275; J. Bolz, U. Ornik, M. Plumer, B.R. Schlei, R.M. Weiner, *Phys. Lett.* **B300** (1993) 404.

[26] N.S. Amelin, R. Lednicky, *Heavy Ion Physics* **4** (1996) 241; SUBATECH 95-08, Nantes 1995, submitted to *Nucl. Phys.* **B**.

[27] B. Erazmus, N. Carjan, D. Ardouin, *Phys. Rev.* **C44** (1991) 2663; B. Erazmus, L. Martin, R. Lednicky, N. Carjan, *Phys. Rev.* **C49** (1994) 349.

[28] M.I. Podgoretsky, JINR Report **P2-85-240** (1985).

[29] W. Zajc, *Phys. Rev.* **D35** (1987) 3396.

[30] W.N. Zhang *et al.*, *Phys. Rev.* **C47** (1993) 795.

[31] S. Pratt, *Phys. Lett.* **B301** (1993) 159.

[32] S. Pratt, *Phys. Rev.* **C50** (1994) 469.

[33] G.F. Bertsch, *Phys. Rev. Lett.* **72** (1994) 2349.

[34] Yu.M. Sinyukov, B. Lorstad, *Z. Phys.* **C61** (1994) 587.

[35] B. Jacak, Proc. Int. Workshop on Multiparticle Correlations and Nuclear Reactions, CORINNE II, Nantes, France, 1994 (ed. J. Aichelin and D. Ardouin, World Scientific, 1994) p. 3.

[36] M. Gazdzicki, *Nucl. Phys.* **A590** (1995) 197c.

[37] Yu.M. Sinyukov, B. Lorstad, V.A. Averchenkov, *Z. Phys.* **C49** (1991) 417.

[38] R. Lednicky, V.L. Lyuboshitz, M.I. Podgoretsky, *Yad. Fiz.* **38** (1983) 251; V.L. Lyuboshitz, *Yad. Fiz.* **53** (1991) 823.

[39] I.V. Andreev, R.M. Weiner, *Phys. Letters* **B253** (1991) 416; Yu.M. Sinyukov, A.Yu. Tolstykh, ITP-92-5E, Kiev, 1992; *Z. Phys.* **C61** (1994) 593.

[40] J. D. Bjorken, Phys. Rev. **D27** (1983) 1327.

[41] Proc. of "Quark Matter 93", *Nucl. Phys.* **A566** (1994).

[42] K. Werner, *Phys. Rep.* **232** (1993) 87.

[43] A. Capella, U. Sukhatme, Chung-I Tan and J. Tran Thanh Van, *Physics Reports* **236** (1994) 225.

[44] A. Kaidalov, *Nucl. Phys.* **A525** (1991) 39c.

[45] H. J. Möhring, A. Capella, J. Ranft, J. Tran Thanh Van, C. Merino, *Nucl. Phys.* **A525** (1991) 493c.

[46] V. D. Toneev, A. S. Amelin and K. K. Gudima preprint GSI-89-52, 1989.

[47] B. Andersen, G. Gustafson and B. Nielsson-Almqvist, *Nucl. Phys.* **B281** (1987) 289.

[48] H. Sorge, H. Stöcker and W. Greiner, *Nucl. Phys.* **A498** (1989) 567c.

[49] F. E. Paige, Lecture at "Theoretical Advanced Summer Institute", Boulder, CO, USA, 1989.

[50] T. Sjöstrand, M. van Zijl, *Phys. Rev.* **D36** (1987) 2019.

[51] X. N. Wang and M. Gyulassy, LBL 31036 (1991), LBL 31159 (1991).

[52] K. Geiger and B. Müller, *Nucl. Phys.* **B369** (1992) 600.

[53] V. A. Abramovskiĭ, V. N. Gribov, O. V. Kancheli, *Sov. J. Nucl. Phys.* **18** (1974) 308.

[54] P. Koch, B. Müller, and J. Rafelski, *Physics Reports* **142** (1986) 167.

[55] U. Heinz, Kang. S. Lee, E. Schnedermann, in "Quark Gluon Plasma", ed. R. Hwa, World Scientific, 1990, page 471.

[56] J. Zimányi, P. Lévai, B. Lucács, and A. Rácz, in "Particle Production in Highly Excited Matter", ed. H.H. Gutbrod and J. Rafelski, Plenum Press, 1993, page 243.

[57] K. Redlich, J. Cleymans, H. Satz, and E. Suhonen, in [41]

[58] H.W. Barz, B.L. Friman, J. Knoll, and H. Schulz, *Nucl. Phys.* **A484** (1988) 661.

[59] L.P. Csernai, J.I. Kapusta, G. Kluge, E.E. Zabrodin, *Z. Phys.* **C58** (1993) 453.

[60] N. Metropolis, A.W. Rosenbluth, M.N. Rosenbluth, A.H. Teller, and E. Teller, *J. Chem. Phys.* **21** (1953) 1087.

[61] Zhang X.Z., D.D.E. Gross, Xu S.H., and Zheng Y.M., *Nucl. Phys.* **A461** (1987) 668.

[62] Klaus Werner and Jörg Aichelin, *Phys. Rev.* **C52** (1995) 1584.

[63] ALICE Technical Proposal., CERN/LHCC 95-71, LHC/P3 (1995), Chapter 11.

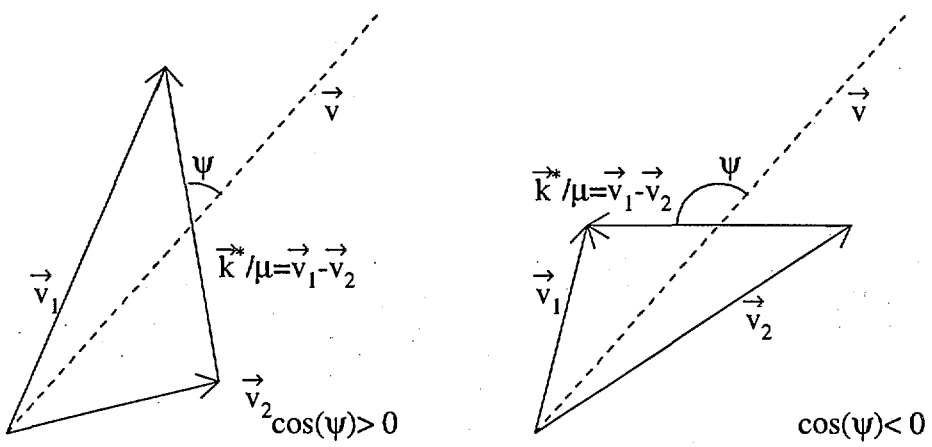

Figure 1: We can determine which sort of particles was produced earlier and which later by studying the correlation functions of two non-identical particles separately for the angles less and greater than 90° between the relative velocity $\mathbf{k}^*/\mu$ ($\mathbf{k}^* = \mathbf{p}_1^* = -\mathbf{p}_2^*$ and μ is the reduced mass of the two particles) and the total pair velocity $\mathbf{v}$.

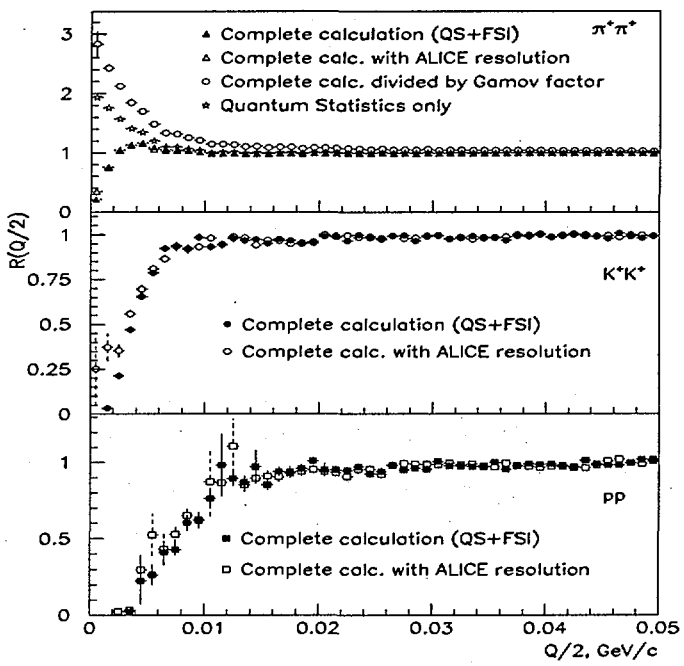

Figure 2: The simulated correlation functions for two identical charged pions, kaons and protons without and with the experimental resolution accounted for. The simulations were done using VENUS model with the extended space-time freeze-out coordinates to set $\langle r \rangle = 30$ fm and $\langle t \rangle = 20$ fm/c in the reaction c.m.s. (scale-factor = 5). For two pions the Gamow corrected correlation function is compared with that including the effect of quantum statistics only.

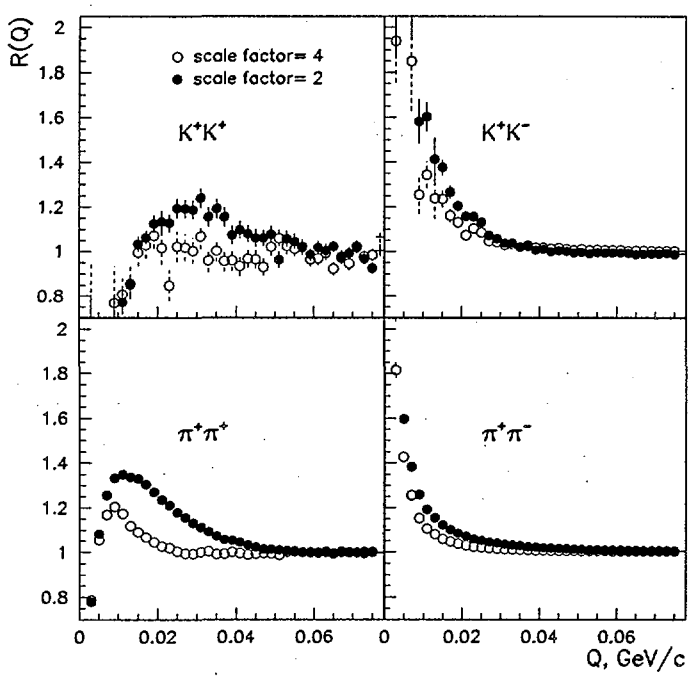

Figure 3: The simulated correlation functions for two like and unlike charged mesons with the experimental resolution accounted for. The simulations were done using VENUS model with the space-time freeze-out coordinates extended by a factor of 2 and 4.

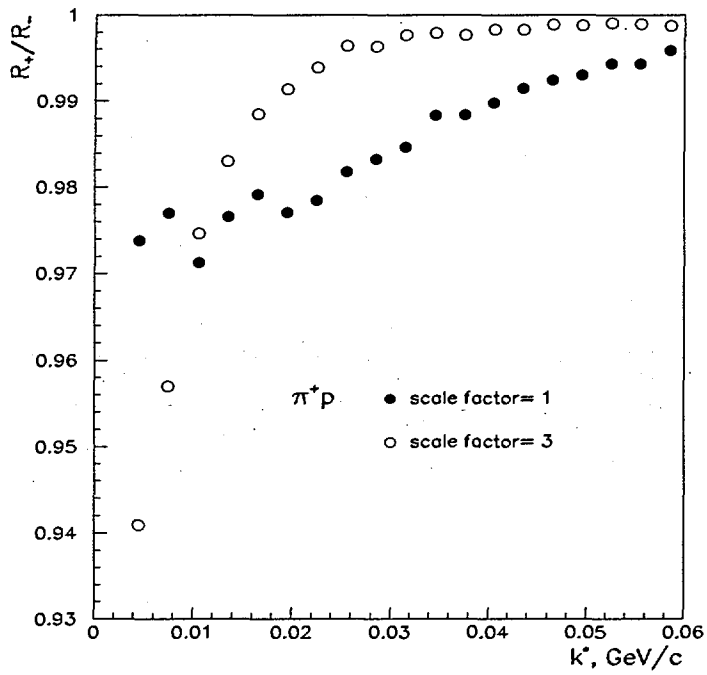

Figure 4: The simulated correlation functions for $\pi^+ p$ pairs with the experimental resolution accounted for. The simulations were done using VENUS model and the same events with 3 times extended space-time freeze-out coordinates.

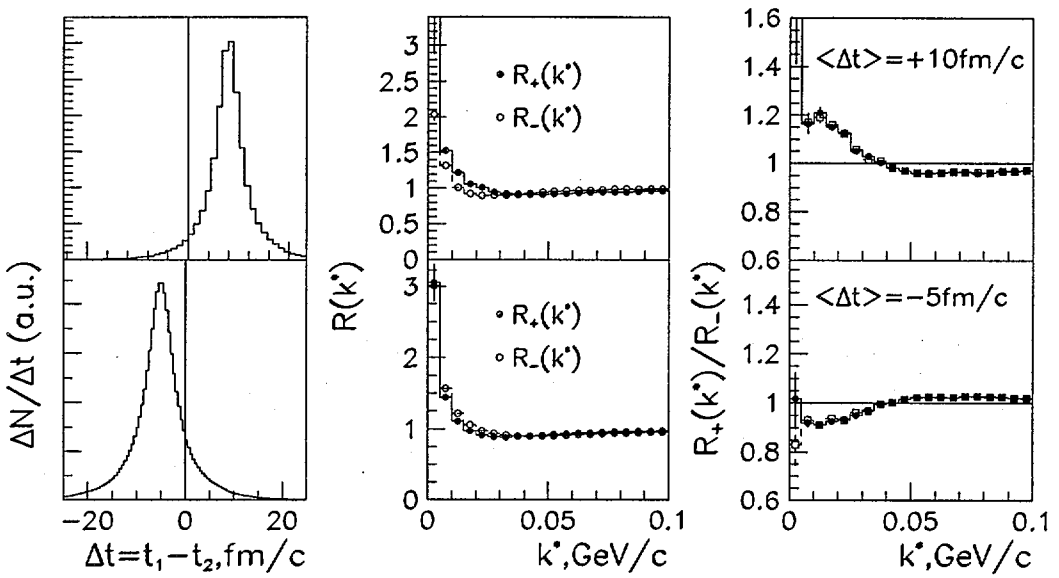

Figure 5: The distributions of the difference of the K^+ and K^- emission times $\Delta t = t_{K+} - t_{K-}$ simulated by VENUS with the shifts $\langle \Delta t \rangle$ =+10 and -5 fm/c introduced *ad hoc* and the corresponding correlation functions R_+ ($\mathbf{v} \cdot \mathbf{k}^* \geq 0$) and R_- ($\mathbf{v}\mathbf{k}^* < 0$) and their ratios calculated for K^+K^- pairs. The ratios distorted by the effect of experimental resolution are represented by open symbols.

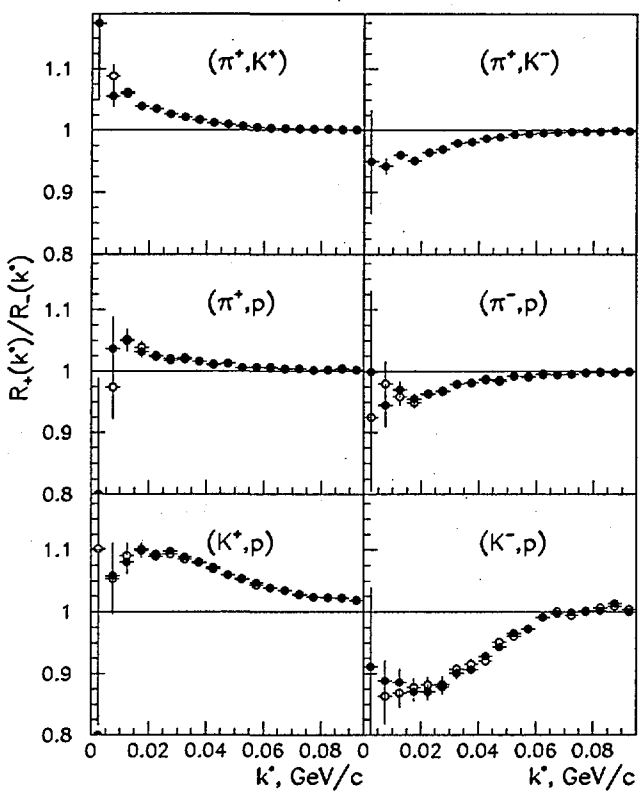

Figure 6: The same ratios R_+/R_- as in Fig. 5 calculated with $\langle \Delta t \rangle$ = -10 fm/c, for different pairs of non-identical particles, taking into account (open symbols) and neglecting (full symbols) the effect of experimental resolution.

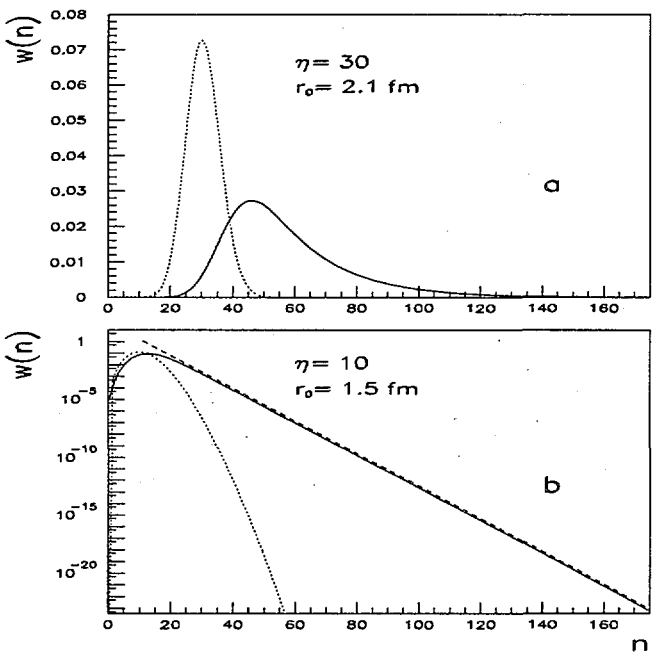

Figure 7: The multiplicity distribution of neutral pions for a) $\Delta = 0.25$ GeV/c, $r_0 = 2.1$ fm, $\eta = 30$ and b) $\Delta = 0.25$ GeV/c, $r_0 = 1.5$ fm, $\eta = 10$, where η is the mean multiplicity of the original Poissonian distributions (dotted curves).

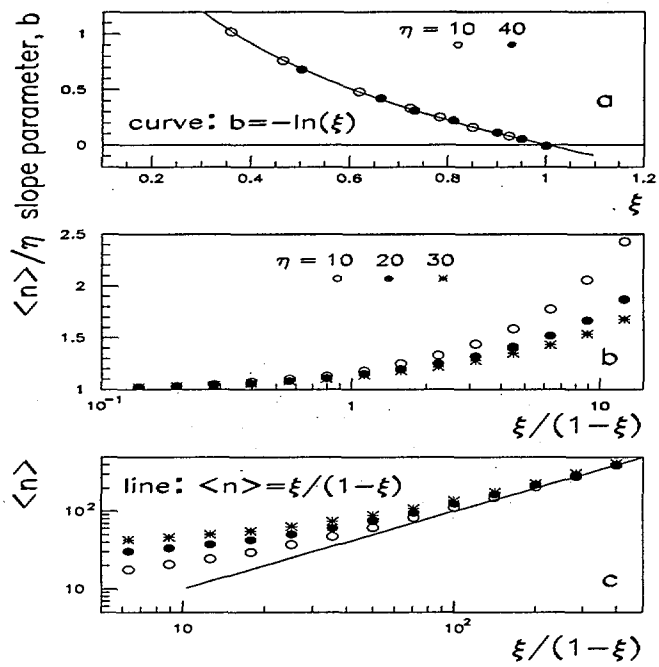

Figure 8: The slope parameter b of the exponential tail $c \cdot \exp(-b \cdot n)$ of the multiplicity distribution (a), the ratio of the mean multiplicity to the original Poissonian one (b) and the mean multiplicity (c) as functions of the density parameters $\xi = \eta/\beta$ and $\xi/(1-\xi)$; $\Delta = 0.25$ GeV/c.

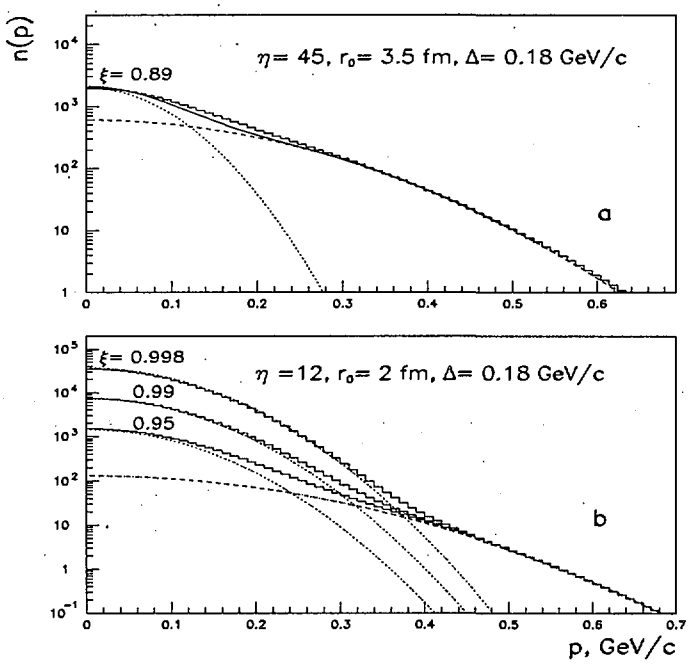

Figure 9: The inclusive single-particle spectra corresponding to the density parameters a) $\xi = 0.89$ and b) $\xi = 0.95$, 0.99 and 0.998 (the corresponding radius r_0 slightly varies near 2 fm). The full curve represents the approximation (47), the dashed and dotted ones - the first and the second term in Eq. (47), respectively.

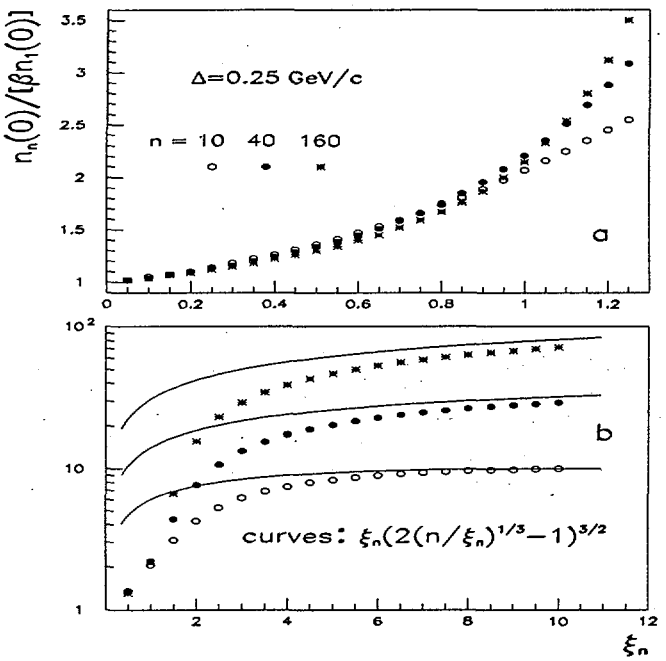

Figure 10: The ratios of the BE affected single-particle spectrum to the dominant large-p contribution $\beta n_1(\mathbf{p})$ of the original spectrum calculated at $\mathbf{p} = 0$ as functions of the density parameter $\xi_n = n/\beta$.

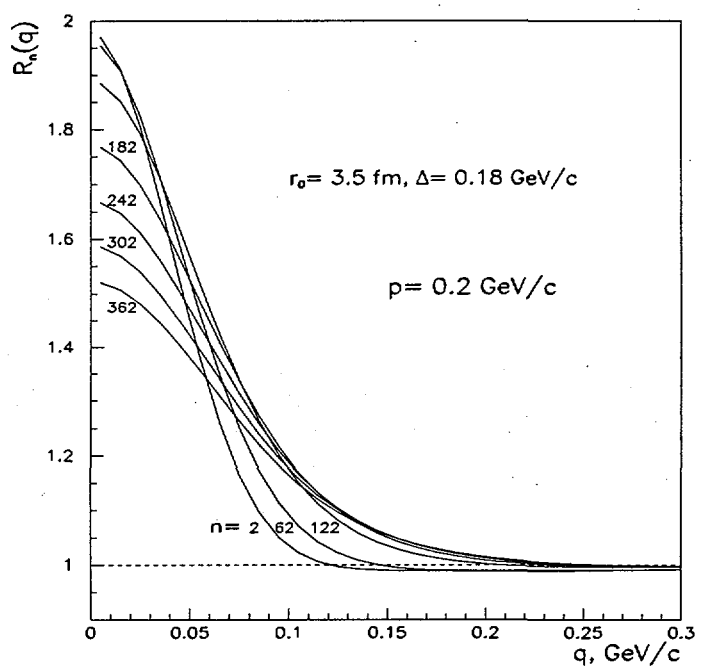

Figure 11: The two-pion correlation functions for the multiplicities increasing from $n = 2$ to 362 with a step of 60 (the corresponding density parameter ξ_n ranging from 0.04 to 7.2 with a step of 1.2). The higher is the multiplicity the lower is the intercept of the correlation function and the larger is its width.

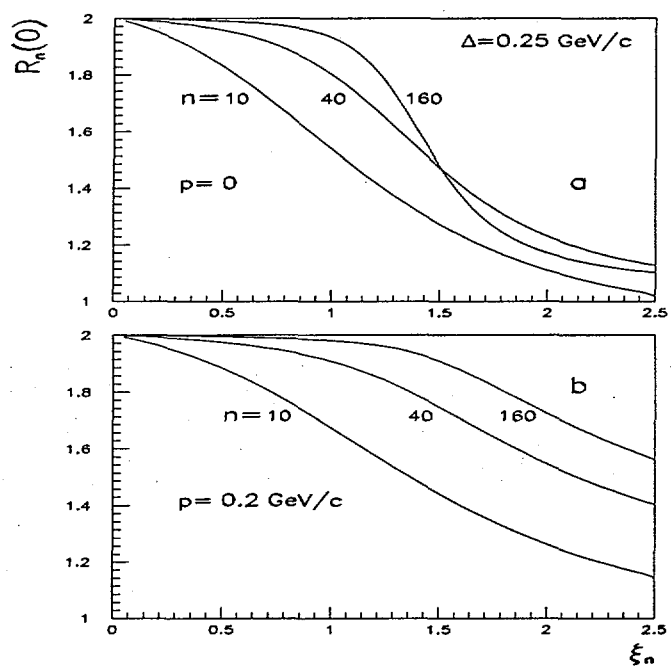

Figure 12: The intercept of the two-pion correlation functions as a function of the density parameter $\xi_n = n/\beta$ for the multiplicities $n = 10$, 40, 160 and for two values $p = 0$ and 0.2 GeV/c of the mean momentum of the two pions.

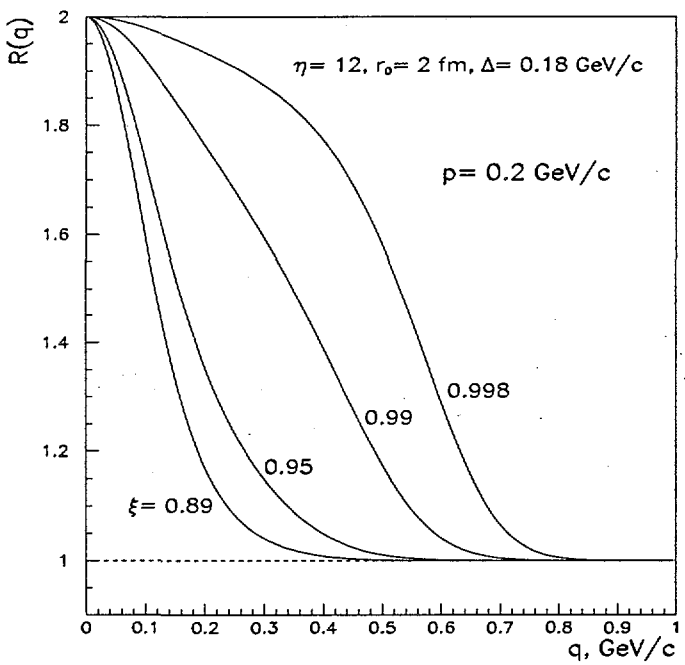

Figure 13: The inclusive two-pion correlation functions demonstrating the increase of the correlation width with the increasing density parameter ξ. The different ξ-values are achieved by slight variations of the radius r_0 around 2 fm.

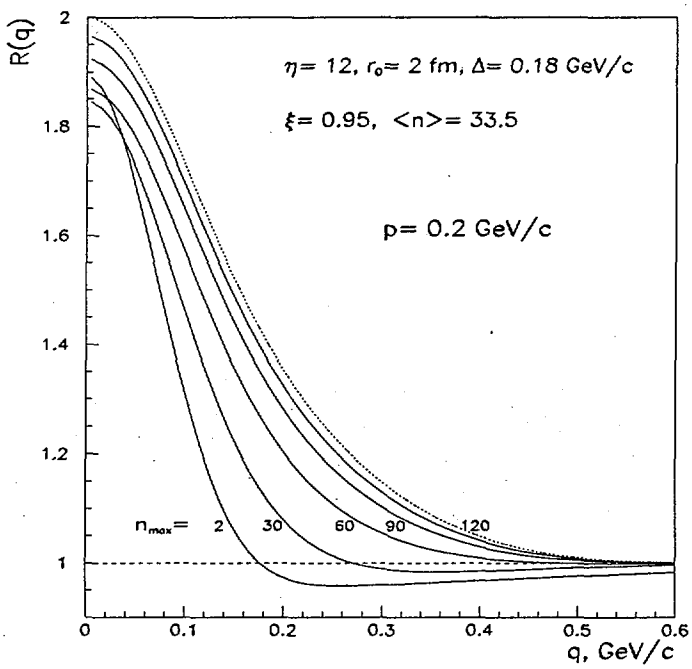

Figure 14: The semi-inclusive correlation functions including the pion multiplicities from 0 to n_{max} for different values of n_{max}. The dotted curve is the inclusive ($n_{max} \to \infty$) correlation function. The conditions are the same as in Fig. 13 for the density parameter $\xi = 0.95$.

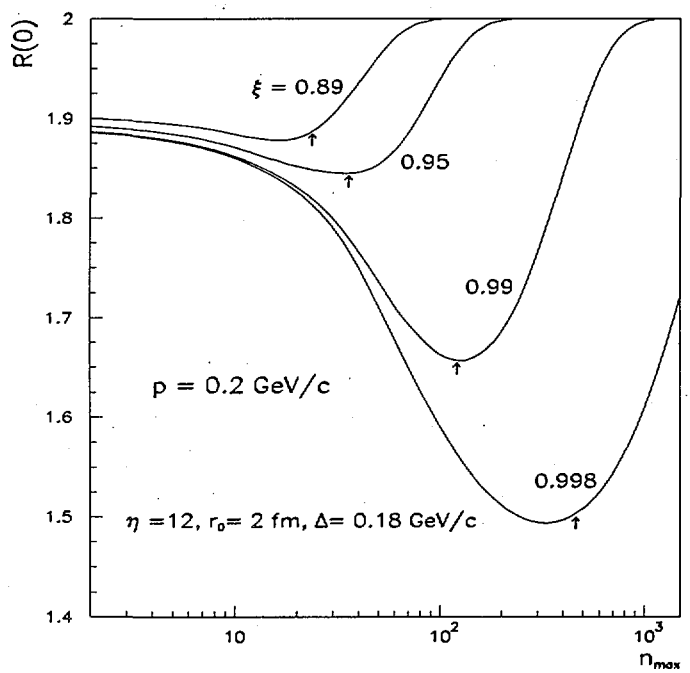

Figure 15: The intercepts of the semi-inclusive correlation function including the pion multiplicities from 0 to n_{max} as functions of n_{max} for different values of the density parameter $\xi = 0.89$, 0.95, 0.99 and 0.998; the arrows indicate the corresponding mean multiplicities $\langle n \rangle = 22.3$, 33.5, 113.7 and 433.8. The conditions are the same as in Fig. 13.